11454–11465 *Nucleic Acids Research, 2018, Vol. 46, No. 21* *Published online 17 October 2018*
doi: 10.1093/nar/gky912

Substrate specificity of human apurinic/apyrimidinic endonuclease APE1 in the nucleotide incision repair pathway

Alexandra A. Kuznetsova[1], Anna G. Matveeva[2,3], Alexander D. Milov[2], Yuri N. Vorobjev[1], Sergei A. Dzuba[2,3], Olga S. Fedorova[1,4,*] and Nikita A. Kuznetsov[1,*]

[1]Institute of Chemical Biology and Fundamental Medicine, Siberian Branch of Russian Academy of Sciences, Novosibirsk 630090, Russia, [2]Institute of Chemical Kinetics and Combustion, Siberian Branch of Russian Academy of Sciences, Novosibirsk 630090, Russia, [3]Department of Physics, Novosibirsk State University, Novosibirsk 630090, Russia and [4]Department of Natural Sciences, Novosibirsk State University, Novosibirsk 630090, Russia

Received July 25, 2018; Revised September 20, 2018; Editorial Decision September 21, 2018; Accepted October 10, 2018

ABSTRACT

Human apurinic/apyrimidinic (AP) endonuclease APE1 catalyses the hydrolysis of phosphodiester bonds on the 5′ side of an AP-site (in the base excision repair pathway) and of some damaged nucleotides (in the nucleotide incision repair pathway). The range of substrate specificity includes structurally unrelated damaged nucleotides. Here, to examine the mechanism of broad substrate specificity of APE1, we performed pulsed electron–electron double resonance (PELDOR) spectroscopy and pre-steady-state kinetic analysis with Förster resonance energy transfer (FRET) detection of DNA conformational changes during DNA binding and lesion recognition. Equilibrium PELDOR and kinetic FRET data revealed that DNA binding by APE1 leads to noticeable damage-dependent bending of a DNA duplex. Molecular dynamics simulations showed that the damaged nucleotide is everted from the DNA helix and placed into the enzyme's binding pocket, which is formed by Asn-174, Asn-212, Asn-229, Ala-230, Phe-266 and Trp-280. Nevertheless, no damage-specific contacts were detected between these amino acid residues in the active site of the enzyme and model damaged substrates containing 1,N6-ethenoadenosine, α-adenosine, 5,6-dihydrouridine or F-site. These data suggest that the substrate specificity of APE1 is controlled by the ability of a damaged nucleotide to flip out from the DNA duplex in response to an enzyme-induced DNA distortion.

INTRODUCTION

Cellular DNA is continually damaged by endogenous and exogenous agents such as highly reactive cell metabolites, external environmental compounds, UV light or ionizing irradiation (1). Recognition and excision of non-bulky DNA base lesions typically proceeds via the base excision repair pathway (BER). The first step in BER is initiated by DNA glycosylases, which locate damaged DNA bases in the large amount of normal DNA. DNA glycosylases catalyse excision of the abnormal base and produce an apurinic/apyrimidinic site (AP-site) (2). Human apurinic/apyrimidinic endonuclease (APE1) is the second enzyme of the BER pathway responsible for the incision of the DNA phosphodiester bond on the 5′ side of AP-sites, thus generating a nick with 3′-hydroxyl and 5′-deoxyribose phosphate termini (3,4). The subsequent steps of the BER pathway resulting in the restoration of the DNA structure are the removal of 5′-deoxyribose phosphate and insertion of the correct nucleotide by a repair DNA polymerase, and finally sealing of the nicked backbone by DNA ligase (5,6).

In the alternative pathway (nucleotide incision repair; NIR), an AP endonuclease makes an incision of the phosphodiester bond on the 5′ side of a damaged nucleotide in a DNA glycosylase-independent manner, resulting in formation of a 3′-OH group and a 5′ dangling damaged nucleotide (7). A number of studies have shown that APE1 recognizes certain types of lesions such as etheno-derivatives of DNA bases (8,9), bulky photoproducts (10), benzene-derived DNA adducts (11), α-anomers of 2′-deoxynucleosides (12), oxidatively damaged pyrimidines (13) and 2′-deoxyuridine (14). Of note, an AP-site and all of these DNA base lesions significantly differ from each other both in the chemical nature of the modification and in the structure of the damaged nucleotide.

*To whom correspondence should be addressed. Tel: +7 383 363 5174; Fax +7 383 363 5153; Email: nikita.kuznetsov@niboch.nsc.ru
Correspondence may also be addressed to Olga S. Fedorova. Tel: +7 383 363 5174; Fax: +7 383 363 5153; Email: fedorova@niboch.nsc.ru

In a number of studies (8–19) the steady-state kinetic parameters for cleavage of DNA containing damaged nucleotides have been reported (Supplementary Table S1). Analysis of the data presented in Supplementary Table S1 reveals that the efficiency of catalytic cleavage of DNA containing various damaged nucleotides most likely decreases in the following order: abasic nucleotide or F-site > 5,6-dihydrouridine > α-adenosine > 1,N6-ethenoadenosine (19–21). It is worth noting that the rate of catalytic hydrolysis (22) and substrate specificity (12,19) of APE1 and its dissociation from a nicked DNA product (23) are modulated by $MgCl_2$ concentration. Therefore, the differences in experimental conditions among various studies could influence the reported efficiency of substrate binding and cleavage.

X-ray crystallographic analysis of human APE1 in the free state (24–26) and in complexes with DNA (27–30) has revealed that this enzyme interacts preferentially with one of the duplex strands usually to form hydrogen bonds and electrostatic contacts between DNA phosphate groups and amino acid side chains or amide groups of peptide bonds of the protein. Residues Arg-73, Ala-74 and Lys-78 contact three consecutive DNA phosphates of the opposing strand on the 5′ side of the AP-site. Residues Tyr-128 and Gly-127 span and widen the minor groove of DNA by ∼2 Å. Formation of enzyme–DNA contacts leads to flipping of an AP site out of the double helix and insertion into the enzyme active site. This site is formed by residues Asp-308, His-309, Glu-96, Asp-70, Asp-210, Tyr-171, Asn-212 and Asn-174. There are only two amino acid residues, Arg-177 and Met-270, inserted into the DNA helix after abasic site eversion. Met-270 is embedded into the DNA minor groove, thereby displacing the base opposite the AP-site. The Arg-177 residue is inserted into the DNA major groove side and forms a hydrogen bond with a phosphate group located downstream of the AP-site. Nonetheless, it has been shown (27) that the M270A enzyme possesses steady-state kinetics similar to those of the wild-type enzyme, whereas the R177A enzyme is significantly faster, indicating that these two residues play uncoupled roles in the course of abasic site eversion and do not equally impact the ability of the enzyme to distort the substrate. In the enzyme–substrate complex that is in a catalytically competent state, a phosphate residue located upstream of the AP-site is coordinated by Asn-174, Asn-212 and His-309 residues. The network of these enzyme–DNA contacts stabilizes the extrahelical conformation of the abasic site, coordinates the scissile 5′-phosphate group in the active site and leads to efficient catalytic hydrolysis of the inter-nucleotide phosphodiester bond.

Of note, structures of complexes of APE1 with matching B-form DNA substrates and products (27–29) have revealed that Watson–Crick base-pairing interactions near the abasic site are preserved. In contrast, the APE1 complex with DNA containing a T/G mismatch 5′ to the AP-site (30) reveals multiple conformers of the substrate, suggesting that DNA undergoes strain while the phosphate backbone gets inserted into the active site. The structural data (27–30) support the hypothesis that the rigid protein core of APE1 induces conformational distortions of the DNA molecule owing to formation of specific contacts that are necessary to achieve the catalytically competent state. According to the suggested mechanism of substrate recognition, correct base-paired DNA flanking of the AP site is needed for formation of specific enzyme–substrate contacts and optimal DNA localization in the active site. Nevertheless, such DNA abnormalities as mismatches prevent the correct binding, thereby reducing the rate of abasic-site cleavage.

Despite the successful characterization of crystal structures of human APE1 bound to a DNA substrate containing an F-site (a stable analogue of a natural AP-site, lacking the hydroxyl group on the C1′ atom of ribose) or a cleaved DNA product, at present, there is no published structure of an APE1 complex with a DNA substrate containing a damaged base. Such structural data could shed light on the nature of the broad substrate specificity of this enzyme.

There are reports of pre-steady-state kinetic analyses of conformational changes in APE1 (19,22,31) and in DNA substrates containing an abasic site (32) or damaged nucleotides such as 5,6-dihydrouridine (DHU) (20) and α-adenosine (αA) (21) in the course of their interactions. Even though APE1 has a rigid protein core, and DNA binding leads to negligible structural rearrangements, changes in the intrinsic Trp fluorescence of the enzyme allowed us here to identify the steps of DNA binding, cleavage and the product release. In this study, it was shown that the rate of hydrolytic cleavage of a DHU-containing substrate (hereafter: DHU-substrate) by APE1 in the NIR pathway is comparable with the rate of cleavage of a DNA substrate containing an abasic site in the BER pathway. Moreover, kinetic assays of conformational dynamics in a stopped-flow fluorescence experiment revealed that APE1 uses the same active site to catalyse the cleavage of DHU- and AP-site-containing substrates (hereafter: AP-substrates). Thermodynamic analysis of the fast stages of recognition and cleavage of DNA containing an abasic site (33) revealed that there are at least two steps of DNA binding and F-site recognition that cause the formation of a catalytically competent complex. Formation of the primary enzyme–substrate complex is characterized by a positive value of standard entropy, which was attributed to desolvation of polar groups in the protein–DNA contact area and a release of highly ordered crystalline water molecules from DNA grooves. This step could include an interaction between the phosphate groups of the DNA duplex from the 5′ and 3′ sides of the F-site and residues Arg-73, Ala-74, Lys-78, Trp-280, Asn-222, Asn-226 and Asn-229. It seems that at this moment, insertion of Arg-177 and Met-270 takes place which is accompanied by displacement of crystalline water from DNA grooves. At the second step of the interaction of APE1 with the F-substrate, a specific rearrangement of the primary complex occurs, which includes eversion of the F-site into the enzyme active centre.

In spite of numerous studies on APE1, the molecular origin of its broad substrate specificity and the mechanism of discrimination between modified bases and/or nucleotides as well as undamaged DNA bases are not yet clear. The substrate specificity to different bases may be associated with different distortions of local DNA structure around the modified base, influencing the efficiency of forming the catalytically active conformation. Another basis for substrate recognition may be related to differences in the efficiency of damaged base eversion, which probably is dependent on the

nature of the base and/or on stability of the damaged base pair in DNA.

The main purpose of our study was to elucidate the key steps of the mechanism behind protein–DNA interaction that ensure highly specific recognition of structurally different damaged nucleotides. In the present work, pulsed electron–electron double resonance (PELDOR) spectroscopy was applied to determine spin–spin distances in spin-labelled DNA duplexes containing the damaged sites in free states and in complex with APE1. Spin labels were attached to the ends of DNA duplexes and did not prevent the protein binding to DNA but enabled sensitive detection of chain bending caused either by a lesion itself or by formation of a complex with APE1. Results of PELDOR measurements were supported by molecular dynamics simulations. Moreover, molecular dynamics revealed the nature of contacts between the active site of the enzyme and various damaged bases. Because of recognition of specific sites in real time accompanied by conformation adjustment of APE1 and DNA to optimize-specific contacts, we performed a pre-steady-state kinetic analysis of conformational changes of APE1 and specific DNA substrates during DNA binding. Real-time conformational rearrangements of DNA during interactions with APE1 were visualized by stopped-flow kinetic assays with Förster resonance energy transfer (FRET) detection. Taken together, our data support the idea that the mechanism of substrate specificity of APE1 is based on the ability of the damaged nucleotide to flip out of the DNA duplex into the active site owing to an enzyme-induced DNA helix distortion and bending.

MATERIALS AND METHODS

Protein expression and purification

To purify APE1 expressed as a recombinant protein, 1 L of culture (in Luria–Bertani [LB] broth) of *Escherichia coli* strain Rosetta II(DE3) (Invitrogen, France) carrying the pET11a-APE1 construct was grown with 50 μg/ml ampicillin at 37°C until absorbance at 600 nm (A_{600}) reached 0.6–0.7; APE1 expression was induced overnight with 0.2 mM isopropyl-β-D-thiogalactopyranoside. The method for isolation of wild-type APE1 was described previously (31,34). The protein concentration was measured by the Bradford method (35); the stock solution was stored at −20°C.

Oligodeoxynucleotides (ODNs)

The sequences of ODNs used in this work are listed in Table 1. The ODNs were synthesized by established phosphoramidite methods on an ASM-700 synthesizer (BIOSSET Ltd., Novosibirsk, Russia) from phosphoramidites purchased from Glen Research (Sterling, VA). α-2′-Deoxyadenosine phosphoramidite was purchased from ChemGenes Corp. (Wilmington, MA, USA). Synthetic oligonucleotides were unloaded from the solid support with ammonium hydroxide according to manufacturer protocols. Deprotected oligonucleotides were purified by HPLC. Concentrations of oligonucleotides were calculated from their A_{260}. ODN duplexes were prepared by annealing modified and complementary strands at a 1:1 molar ratio.

Table 1. DNA sequences and structures of lesions introduced into the DNA duplexes*

Shorthand	Sequences of DNA duplexes
X-substrate X = F-site, DHU, εA, αA or A	5′-TCTCTC**X**CCTTCC-3′ 3′-R-AGAGAGCGGAAGG-R-5′
FAM-Y-substrate	5′-**FAM**-GCTCA**Y**GTACAGAGCTG-3′
Y = F-site, DHU, εA, αA	3′-CGAGTGCATGTCTCGAC-**BHQ1**-5′

*R is 4-amino-2,2,6,6-tetra-methylpiperidine-1-oxyl phosphate, FAM is 6-carboxyfluorescein, BHQ1 is black hole quencher.

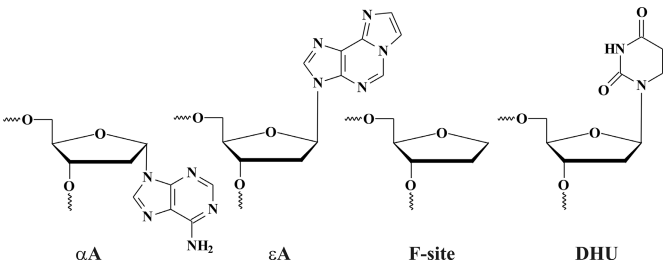

Sample preparation

The DNA duplexes for PELDOR measurements were obtained by mixing of single-stranded oligonucleotides (undamaged or containing lesion) with a complementary 4-amino-2,2,6,6-tetramethylpiperidine-1-oxyl deoxyribooligonucleotide sequence at room temperature in binding buffer consisting of 10 mM Na_2HPO_3 (pH 7.5) and 140 mM NaCl. As a cryoprotective solvent, we used a deuterated water/deuteroglycerol mixture at 1:1 (v/v). The concentrations of spin-labelled DNA were 2.5×10^{-4} M. Approximately 25 μl of a DNA solution was placed in quartz tubes of a 0.3 cm inner diameter. After freezing in liquid nitrogen, the solutions formed transparent glass. At all stages of the synthesis and sample preparation, special care was taken to prepare the solutions under the same conditions (e.g. purification procedures, dissolving).

Samples containing the APE1 protein were prepared by dilution of an appropriate concentration of the DNA substrate with a stock solution of the protein. The final concentrations of spin-labelled DNA and APE1 were 1.5×10^{-4} M.

PELDOR measurements

PELDOR measurements were carried out on an X-band Bruker ELEXSYS E580 EPR spectrometer equipped with a split-ring Bruker ER 4118 X-MS-3 resonator. A three-pulse PELDOR setup was employed, with the microwave pulse sequence $\pi/2$– *T–pumping pulse*–(τ-*T*)–π –τ– *echo*, where the pumping pulse is applied at a different frequency. The pulse lengths of the $\pi/2$ and π echo-forming detection pulses were 16 and 32 ns, respectively. The pumping pulse duration was 28 ns, its amplitude was chosen to provide the maximal influence on the detected echo signal. The pumping pulse was applied in all cases at frequency ν_B corresponding to the maximum of an echo-detected electron paramagnetic resonance (EPR) spectrum. The difference

$\nu_A - \nu_B$ between the detection and pumping frequencies was kept at 65 MHz. The resonator was cooled within an Oxford Instruments CF-935 cryostat with flowing cold gaseous nitrogen. The sample temperature was kept near 80 K.

Because we used a deuterated solvent, we were able to extend the accessible range for the delay T variations by setting delay τ between two detection pulses as large as 7 μs. Delay T was scanned with a step of 32 ns, starting from the negative initial delay d_0 = –200 ns. Starting delay T for the PELDOR time trace analysis (T = 0) was determined as described in ref. (36). The echo signal was integrated with a time gate of 80 ns. The signal distortion, occurring after the pumping pulse passage through the detecting pulses, was corrected as described in Ref. (37).

During PELDOR data processing, to obtain the distance distribution function $P(r)$ between two spin labels in the DNA molecule, three approaches were employed: the conventional Tikhonov regularization approach (DeerAnalysis2013) (38), and two novel methods: multi-Gaussian regularization (39) and Mellin transformation (40).

Stopped-flow fluorescence measurements

Stopped-flow measurements with fluorescence detection were carried out mostly as described elsewhere (41,42). In brief, we used a SX.18MV stopped-flow spectrometer (Applied Photophysics Ltd, UK) equipped with a 150 W Xe arc lamp and an optical cell with 2-mm path length. The dead time of the instrument is 1.4 ms. The fluorescence of Trp was excited at λ_{ex} = 290 nm and monitored at λ_{em} > 320 nm as transmitted by filter WG-320 (Schott, Mainz, Germany). Fluorescence of a 6-carboxyfluorescein (FAM) residue was excited at λ_{ex} = 494 nm and monitored at λ_{em} > 515 nm as transmitted by filter OG-515 (Schott, Mainz, Germany). Trp fluorescence detection experiments were conducted with catalytically active APE1 at 25°C in a buffer consisting of 50 mM Tris–HCl pH 7.5, 50 mM KCl, 1.0 mM ethylenediaminetetraacetic acid (EDTA), 1.0 mM dithiothreitol, 0.1 mM $MgCl_2$ and 7% glycerol (v/v). Registration of the DNA binding process by means of a FRET signal was carried out in the absence of Mg^{2+} ions with catalytically inactive apo-APE1 at 25°C in a buffer consisting of 50 mM Tris–HCl pH 6.8, 50 mM KCl, 1.0 mM EDTA, 1.0 mM dithiothreitol and 7% glycerol (v/v).

APE1 was placed in one of the instrument's syringes and rapidly mixed in the reaction chamber with the DNA substrate from another syringe. The concentrations of the DNA substrate and APE1 in all the experiments were 1.0 μM. The reported concentrations of reactants are those in the reaction chamber after mixing. Typically, each trace shown in the figures is the average of four or more fluorescence traces recorded in individual experiments.

Conformational changes in the protein were monitored by changes in Trp fluorescence intensity. In the case of εA-substrate, total emission of Trp and εA fluorescence were registered. The FAM-Y-substrates modified at 5′ termini with the dye-quencher pair FAM/BHQ1 (Table 1) were subjected to Förster resonance energy transfer (FRET) measurements. FRET analysis revealed changes in the distance between the dye and quencher in the processes of DNA helix distortion during formation of the APE1–DNA complex. Because of the influence of damaged nucleotides on the length of the free DNA duplexes, the distances between FRET dyes in these duplexes in the free state were different. In the figures, for better presentation, the curves were manually moved apart. This procedure does not affect the results of fitting because the background fluorescence is fitted separately for each curve.

Polyacrylamide gel electrophoresis (PAGE) enzyme assays

Single-turnover APE1 endonuclease assays were performed in a reaction buffer composed of 50 mM Tris–HCl pH 7.5, 50 mM KCl, 1.0 mM EDTA, 1.0 mM dithiothreitol, 0.1 mM $MgCl_2$ and 7% glycerol (v/v). The reaction solution contained 1.0 μM APE1 and 1.0 μM DNA substrate. The reactions were carried out at 25°C for 10 min and quenched by a gel-loading dye containing 7 M urea and 50 mM EDTA, and then loaded on a 20% (w/v) polyacrylamide gel containing 7 M urea. Disappearance of the substrate and formation of the product were analysed by autoradiography and quantified by scanning densitometry in the Gel-Pro Analyzer software, v.4.0 (Media Cybernetics, USA).

Fitting of stopped-flow data

The initial part of Trp fluorescence and FRET stopped-flow kinetic traces were fitted to Equation (1) by a nonlinear regression procedure in the Origin software (OriginLab Corp., USA):

$$F = F_b + \sum_{i=0}^{N} A_i \times \exp(-k_i \times t), \quad (1)$$

where F is the observed fluorescence intensity of Trp or FAM, F_b is the background fluorescence, A_i represents fluorescence parameters, k_i denotes the observed rate constant, and t is the reaction time.

Molecular modelling

Molecular modelling of the APE1 complex with 13 nt DNA duplexes containing 1,N6-ethenoadenosine, α-adenosine, 5,6-dihydrouridine or F-site (Table 1) included several stages: (i) building up an initial atomic structure of a complex, (ii) refinement of atomic structure of the complex by energy optimization and simulated annealing, (iii) productive modelling of molecular dynamics of each complex and accumulation of a representative set of instant structures along an equilibrated molecular dynamics trajectory.

Initial structure of APE1–DNA complexes. To build an initial structure of APE1–DNA complexes, containing the required 13 nt sequences with DHU, εA, αA or F-site, the X-ray APE1–DNA complex (PDB ID: 1DE8) was employed as a template. DNA sequence in structure 1DE8 was replaced by respective 13 nt DNA duplexes containing an F-site (F-substrate). Such replacement can be done with a moderate deformation of the ribose-phosphate backbone atomic structure, because distances C1′–C1′ for G:C and A:T base pairs are equal within a fraction of 1 Å.

The APE1–DHU-substrate complex was constructed by replacement of the F-site by 5,6-dihydrouridine (Table 1). Atomic structures of complexes with εA- and αA-substrates were built by similar approach with use of *slow-grow* and *soft-core* techniques (43,44). Finally, the spin labels were added to obtain initial atomic structure of experimentally used DNA substrates.

Refinement of the atomic structure of APE1–DNA complexes. An initial structure of a complex of APE1 with a DNA substrate was energy optimized and then optimized by the method of molecular dynamics using the soft-core option of the BioPASED software (43,44). The soft-core method allows atoms to have a soft interaction between atoms at small interatomic distances; this method was developed to find an optimal docking mode of a large flexible drug molecule on a given protein (43).

Productive modelling of APE1–DNA complexes by molecular dynamics. Final optimization of the structure for the complex of APE1 with a DNA substrate was performed by molecular dynamics in the BioPASED software (44). BioPASED calculates a molecular dynamic trajectory of a protein–DNA complex in the NVT ensemble using a multiple time step integrator and a twin range pair list for van der Waals and electrostatic interactions (45). The BioPASED software uses Amber all-atom force field ff99 for proteins in conjunction with the general Amber force field (GAFF) (45–47) for modified nucleic base atoms. Amber force field ff99 has parameters for a small set of organic molecules and thus is not widely used in studies of ligand–protein interactions, whereas the GAFF works for most of pharmaceutical molecules, and is designed to be compatible with Amber force field ff99. Atomic charges of modified nucleic base atoms were calculated by the charge equalization method (48). The original GS model was extended to describe solvation of nucleic acids and proteins (44). The protocol of simulations that was applied to all four APE1–DNA substrate complexes consisted of three stages: (i) structure relaxation by 500 cycles of conformational energy minimization by the method of biconjugated gradients; (ii) slow heating of the system from the initial temperature of 5 K to room temperature (300 K) during 500 ps, with a time step of 0.001 ps (target temperature of the Berendsen thermostat was increased by 0.002 K for each time step); (iii) system equilibration at a constant temperature of 300 K with the Berendsen thermostat during 500 ps; (iv) a productive simulation of 10 ns duration for each complex at a constant temperature of 300 K.

The equilibrium 10 ns molecular dynamic trajectories were analysed to compute end-to-end distance distribution between oxygen atoms at 5′ and 3′ ends of a damaged DNA strand and between oxygen atoms of spin label 4-amino-2,2,6,6-tetra-methylpiperidine-1-oxyl (Table 1).

RESULTS

Rationale

Most of the biological importance of APE1 in the DNA repair pathways is associated with the high affinity for the abasic nucleotide and nicking of DNA hydrolytically 5′ to the AP-site. Nevertheless, the ability of APE1 to incise the DNA sugar–phosphate backbone 5′ to structurally unrelated lesions such as α-anomeric 2′-deoxynucleosides, various red/ox-modified pyrimidines and etheno-adducts has been demonstrated in a number of studies published over the past 15 years (8–14).

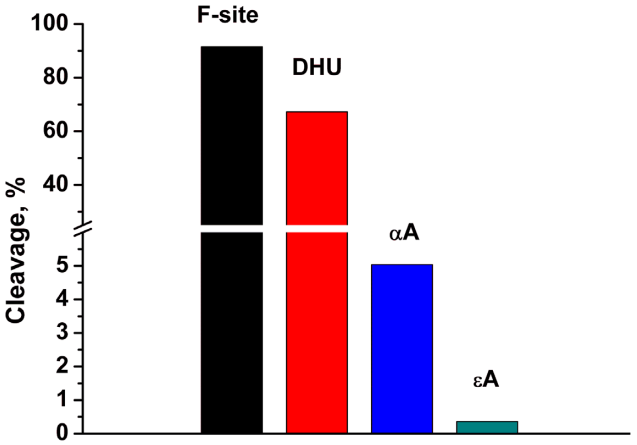

Figure 1. Dependence of the cleavage extent on the nature of a damaged nucleotide. [APE1] = [DNA substrate] = 1.0 μM, [$MgCl_2$] = 0.1 mM.

In the present study, to elucidate the mechanism of the substrate discrimination by APE1, we analysed model DNA duplexes containing as specific lesions an F-site, 5,6-dihydrouridine, α-anomer of adenosine or 1,N6-ethenoadenosine. To compare these DNA substrates, equilibrium and kinetics approaches as well as molecular dynamics simulation were used. Direct detection of the product formation by polyacrylamide gel electrophoresis (PAGE) allowed for estimating the efficiency of enzymatic hydrolysis of different double-stranded DNA substrates under the same experimental conditions. PELDOR analysis of the enzyme–substrate mixture in the equilibrium state revealed damage-dependent DNA duplex bending in the complex with the enzyme. Real-time conformational rearrangements of the enzyme and DNA during their interactions were visualized by the stopped-flow kinetic assays. The nature of the contacts between a damaged base and amino acids of the active site of the enzyme was determined in the molecular dynamics simulation. Finally, the structural basis for the substrate specificity of APE1 will be discussed.

DNA cleavage efficacy by APE1

Under the same conditions and $MgCl_2$ concentration, the efficiency of enzymatic hydrolysis of double-stranded DNA substrates containing modified nucleotides was estimated by PAGE (Figure 1). Direct detection of the product formation enables ranking the efficiency of DNA substrate cleavage in the following order: F-site > DHU >> αA > εA, in accord with earlier studies (19–21).

PELDOR measurements of the end-to-end distance

Conventional EPR spectra and original PELDOR time traces of the analysed systems were similar to those

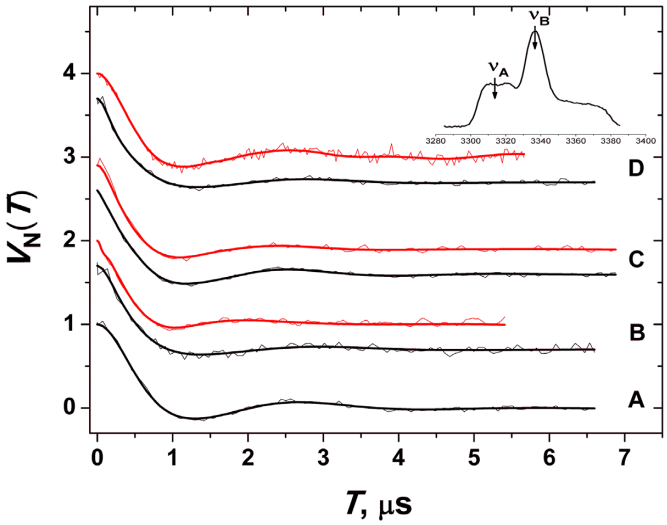

Figure 2. Experimental PELDOR time traces (noisy curves) and their simulations (solid curves) using multi-Gaussian regularization (see text). (**A**) An undamaged DNA duplex, (**B**) DHU-substrate and its complex with APE1 (the curve shifted upwards), (**C**) the same for αA-substrate, (**D**) the same for εA-substrate. The inset shows the frequency position of the detection (ν_A) and pumping (ν_B) microwave pulses in the ESE-detected EPR spectrum.

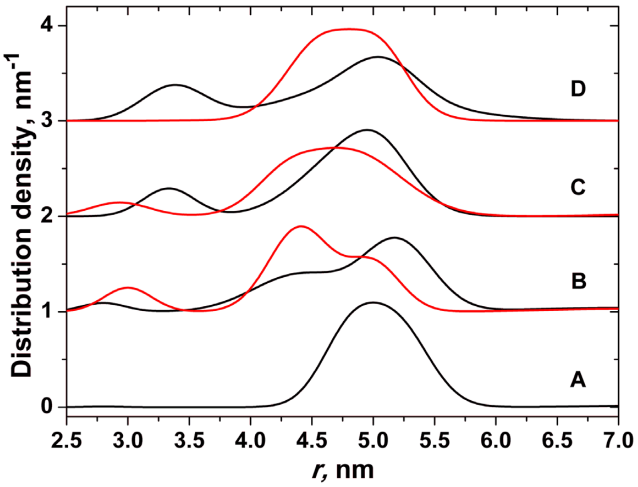

Figure 3. The distance distribution functions obtained by multi-Gaussian regularization for free DNA duplexes (black curves) and complexes with APE1 (red curves). (**A**) Control undamaged DNA duplex, (**B**) DHU-substrate, (**C**) αA-substrate, (**D**) εA-substrate.

presented previously (36,49). The PELDOR traces contain a contribution from inter-molecular magnetic dipole–dipole interactions between spin labels of different DNA molecules and a contribution from intra-molecular interactions between two spin labels in the same DNA molecule. The inter-molecular contribution was removed from the experimental time traces in the way it was done in refs. (36,49), and the refined intramolecular contribution to the PELDOR signal, $V_N(T)$ was thus obtained (Figure 2).

The distance distribution function reflecting the probability of realizing each particular distance was obtained via three approaches. Because of the ill-posed nature of the mathematical problem when the distance distribution function is obtained from experimental time traces (38), a combination of different approaches can provide more reliable information. It was found that all these approaches are in similarly good agreement with the experimental curve as it is shown in Figure 2 for only one of them. Moreover, the obtained distance distribution functions look alike (Supplementary Figure S1) indicating the accuracy of calculations for large distances.

Figure 3 shows the distance distribution functions obtained by the multi-Gaussian approach, which is more convenient when different distributions are superimposed, and it is necessary to estimate their proportion. Typically, three or four Gaussians were employed to model the distance distribution (39). From the data in Figure 3, the r_{max} values were found (Table 2). The portion of DNA molecules belonging to a particular r_{max} was simply estimated by adding amplitudes of the Gaussians contributing to this maximum. In addition, in Table 2, the results of r_{max} estimation via conventional Tikhonov regularization and Mellin transformation are given (see Supplementary Figure S1). The difference between different approaches may be attributed to uncertainties in the determination of r_{max} as a result of the ill-posed problem mentioned above.

One can see that the positions of the main maximum of all DNA duplexes in the free state are close to 5.0 nm (Table 2) and are in line with the previously obtained data for undamaged DNA (49). A comparison of distances in the APE1–DNA complexes revealed that under these experimental conditions, DNA duplexes partially remain in a free state with a distance of ∼5.0 nm, along with emergence of a substantial amount of conformations with smaller distances. These distances between spin labels decrease in the order DHU < αA < εA (Figure 3 and Table 2).

The appearance in some cases of an additional small maximum at 3.3 nm is strongly influenced by the method employed in the PELDOR data analysis (Supplementary Figure S1B and C). Therefore, this phenomenon may be, at least partly, an artefact caused by the ill-posed nature of the mathematical problem underlying this analysis.

The obtained distances allowed us to calculate the DNA bent angle induced by a damaged nucleotide itself or induced by binding to APE1 by means of the formula $\cos\Theta = (r^2 - r_1^2 - r_2^2)/(2 \times r_1 \times r_2)$, where r is the distance between two labels, and r_1 and r_2 are distances between labels and the central damaged nucleotide (Supplementary Figure S2). For simplicity, it was taken into account that $r_1 = r_2 = r_0/2$, where r_0 is the distance between two spin labels in the undamaged duplex in the free state.

Kinetic analysis of DNA binding. To ascertain the efficacy of enzyme–substrate complex formation, the kinetics of APE1 binding to a damage-containing DNA duplex were analysed by the stopped-flow method. The Trp fluorescence traces of APE1's reaction with the DNA substrates comprised the characteristic decrease and increase phases (Figure 4A), which previously (19,22,31) were assigned to DNA-binding steps and the catalytic reaction, respectively, (for an F-substrate). A comparison of kinetic traces obtained for damaged-base-containing DNA substrates re-

Table 2. Parameters of the distance distribution obtained by multi-Gaussian regularization (MGR), Tikhonov regularization (TR) or Mellin transformation (MT)

Sample	r_{max}, nm (MGR)	Portion,[a] %	r_{max}, nm (TR)	r_{max}, nm (MT)	Angle of DNA kinking
Undamaged DNA	5.0	100	5.0	5.0	0
F-substrate[b]			4.83		20
DHU-substrate	4.5	37	4.4		57.4
	5.2	51	5.0	5.1	
αA-substrate	4.95	84	5.0	4.9	18
εA-substrate	4.95	76	5.0		18
DHU-substrate/APE1	4.4	67	4.4	4.4	63.0
	4.9	28	4.9	4.9	25.5
αA-substrate/APE1	4.7	88	4.7	4.7	44.3
εA-substrate/APE1	4.8	100	4.9	4.9	36.1

[a]In some cases, the sum is not exactly 100% because of a small admixture of unrealistically short or large r_{max} in the results of simulation.
[b]From Ref. (49).

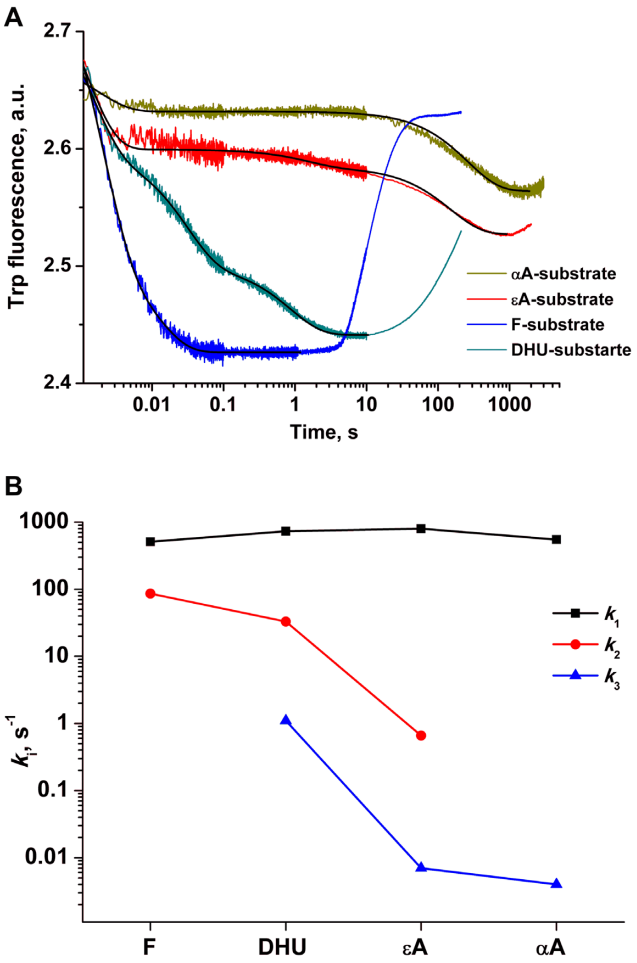

Figure 4. (**A**) Stopped-flow Trp fluorescence kinetic traces. (**B**) Values of observed rate constants k_i determined by Equation (1) ($i = 2$ or 3).

vealed an initial decrease of the Trp fluorescence intensity in all cases. Nevertheless, in the case of the F-substrate, a visual single-phase drop of Trp fluorescence intensity was detected and was attributed to the process of formation of a specific enzyme–substrate complex. In the cases of DHU-, αA- and εA-substrates, a slow second decrease phase appeared, with the characteristic time of Trp intensity drop off increasing in the order F-site < DHU < αA ≈ εA. Appearance of the increase in the Trp fluorescence intensity at the end of kinetic traces characterizes the beginning of the catalytic reaction. The decrease phases of Trp fluorescence kinetic traces were fitted to a double-exponential equation (F- and αA-substrates) or a triple-exponential equation (DHU- and εA-substrates) (Equation 1, $i = 2$ or 3), respectively. The values of the observed rate constants for all DNA substrates were plotted as presented in Figure 4B. As follows from Figure 4B, the observed rate constant k_1 of the first fast phase is weakly dependent on the nature of the damaged nucleotide. Nevertheless, rate constants of the second and third decrease stages significantly decreased in the case of DNA duplexes containing a damaged base. It was previously shown (33) for an F-substrate that the initial step of the DNA substrate binding includes formation of non-specific contacts between the enzyme's binding surface and DNA. The second binding step involves the F-site flipping-out process and formation of specific contacts between the enzyme active site and the everted 5′-phosphate-2′-deoxyribose residue. The obtained data revealed that eversion of the nucleotide with a damaged base depends on the nature of the lesion, proceeds more slowly in comparison with the F-site and splits into two phases in the kinetic trace in cases of DHU and εA.

To characterize the DNA distortion processes in the course of enzyme–DNA complex formation, dye-labelled FAM-Y-substrates were subjected to FRET analysis. In the stopped-flow kinetic trace obtained during the interaction of APE1 with a DNA substrate containing a damaged base, the initial increase in the FRET signal (up to 10 ms) was followed by a decrease (Figure 5A). The initial growth reflects some DNA duplex distortion in the course of non-specific complex formation and is in line with the changes detected by Trp fluorescence assays. Interaction of APE1 with the FAM-F-substrate was characterized by a single decrease in the fluorescent signal in the time range up to 0.1 s, suggesting that in the case of the F-site, initial DNA distortion proceeds too fast and occurs during the dead time of stopped flow mixing ($\tau = 1.4$ ms; Figure 5A). The drop off in the FRET signal reflects the decrease in the distance between FAM and quenching BHQ1 residues because of DNA bending in the complex with APE1.

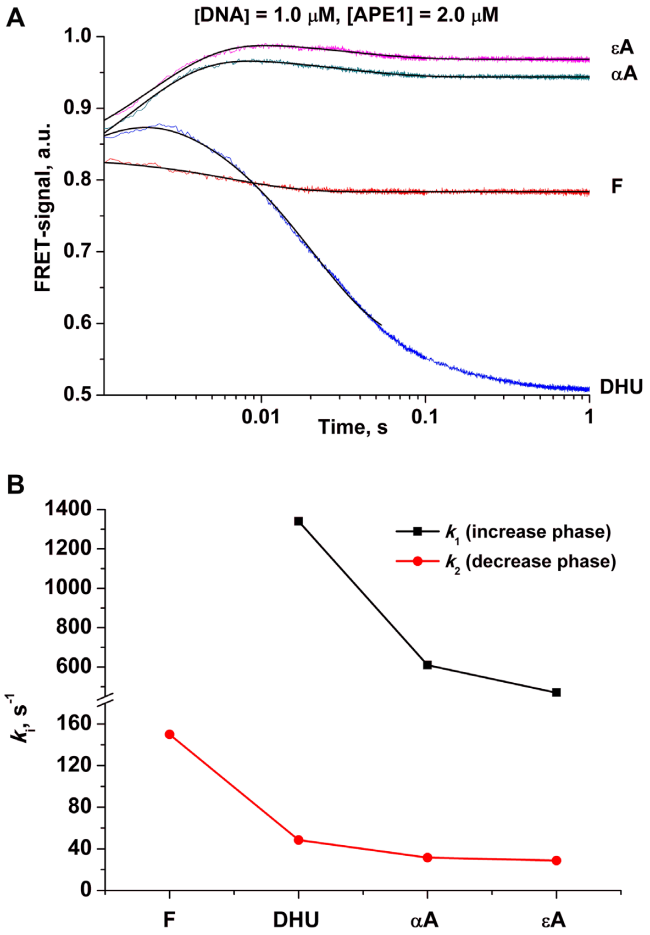

Figure 5. (**A**) FAM/BHQ1 FRET traces of the interaction of APE1 with the FAM-Y-substrates. (**B**) Values of the observed rate constants k_i determined via Equation (1) ($i = 1$ or 2).

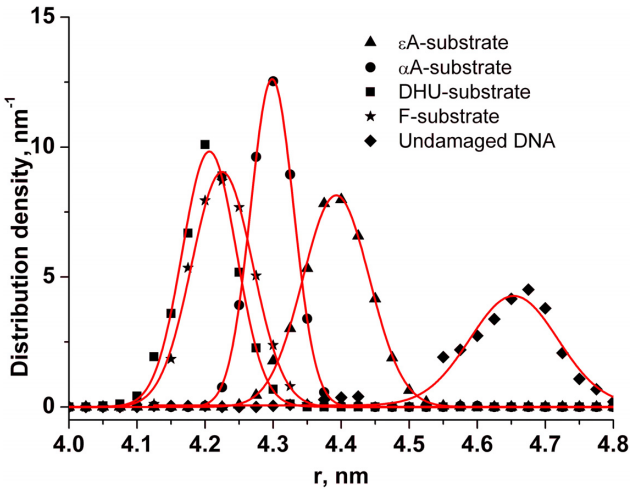

Figure 6. The distribution of end-to-end distances in the APE1–DNA complexes obtained by the molecular dynamics simulation. A DNA duplex containing an F-site (stars), DHU (squares), αA (circles) or εA (triangles). The smooth red curves were calculated using the Gaussian function.

An exponential fit of the kinetic traces to Equation (1) ($i = 1$ or 2) enabled us to compute the observed rate constants of both phases (Figure 5B). The observed rate constants of the increase phase can be ranked in the order F-site > DHU > αA > εA. Of note, conformational changes of APE1 detected by Trp fluorescence revealed approximately the same observed rate constants of initial binding, suggesting that conformational adjustment of a DNA duplex proceeds after changes in the enzyme and strictly depends on the nature of the damaged nucleotide. Observed rate constants k_2 of DNA bending at the decrease step are also damaged-base-dependent and diminish in the order F-site > DHU > αA > εA.

Molecular dynamics simulations. Preliminary optimized structures of APE1 complex with four modified DNA substrates where equilibrated within 10 ns to stabilize total potential energy of complex (Supplementary Figure S3). Then equilibrium 10 ns molecular dynamics trajectories were generated at room temperature (300 K) for each APE1–DNA complex to collected end-to-end distance dynamics (Supplementary Figure S4). The obtained distance distribution functions are depicted in Figure 6. The distance distributions were fitted to a Gaussian function to calculate positions of the maxima, r_{max}, and the width at the half-height, Δ, obtained for all samples (Table 3). Readers can see that distances between the 5′-end O atom and 3′-end O atom decrease in the order F-site, DHU < αA < εA. Moreover, fluctuations of the distances did not exceed 0.1 nm, indicating stable DNA conformation in the enzyme–DNA complex. Angles of DNA kinking in the complex with APE1 are in agreement with PELDOR measurements with decreasing values at 6–7°. Of note, the reported angles of DNA bending in X-ray structures of APE1 with an F-site–containing DNA are equal to 35° (27,30).

As demonstrated in another study (49), spin labels attached to the phosphate groups of 5′ or 3′ end of the duplexes via a linker that has three (P–O5′, O5′–C5′, C5′–C4′) or two (P–O3′, O3′–C3′) bonds is capable of internal rotation. These flexible linkers provide a lot of freedom to the spin-labelled fragment, relative to the DNA duplex. In the case of enzyme–DNA complexes, rotation of the spin labels can be spatially restricted or stabilized in some fixed conformations by interaction with a protein surface. Indeed, the distribution of distances between active oxygen atoms of spin labels revealed large fluctuation with several maxima. As an example, Supplementary Figure S5 presents end-to-end distance distribution of the APE1–DHU-substrate complex, which was fitted to a double Gaussian function. Furthermore, flexibility of spin labels causes the appearance of short distances ($r_1 = 3.7$ nm and a large value of the width at the half-height, $\Delta_1 = 0.7$ nm) in the MD distribution. Moreover, the maximum of the second Gaussian $r_2 = 4.5$ nm is close to the distance of the bent state of the DHU-substrate (Table 2).

A model structure of a damaged nucleotide-binding pocket

The APE1–DNA complexes with minimal total energy were selected from the molecular dynamic trajectories to get insight into the structure of the damaged nucleotide-binding pocket. A comparison of structures among DNAs contain-

Table 3. Modelled end-to-end distances between terminal atoms for DNA duplexes in complex with APE1

	r_{max}, nm	Δ, nm	Angle of DNA kinking
Undamaged DNA	4.65	0.1	NA
F-site	4.22	0.09	55
DHU	4.21	0.08	56
αA	4.30	0.06	50
εA	4.4	0.1	42

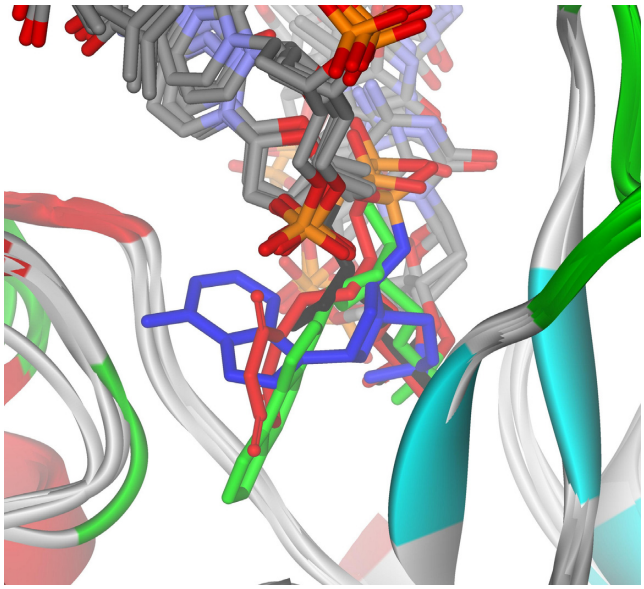

Figure 7. Superposition of the structures of APE1's binding pocket adapted for an F-site (black), DHU (red), εA (green) or αA (blue).

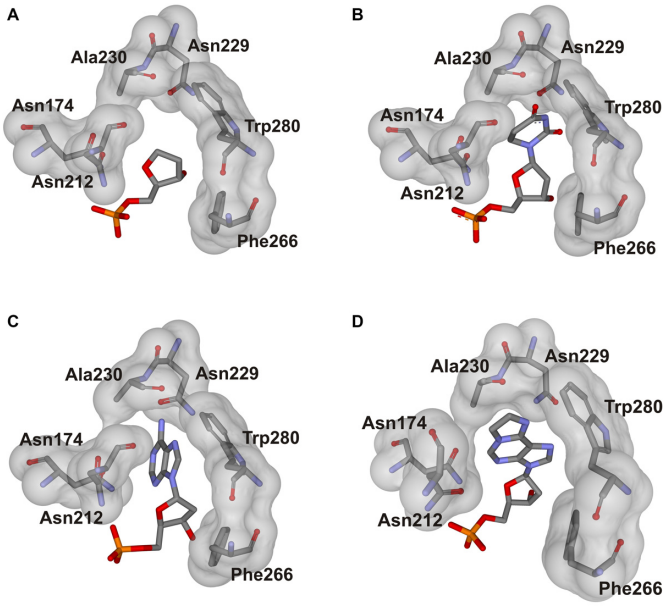

Figure 8. Close-up view of APE1's binding pocket containing a damaged nucleotide: F-site (**A**), DHU (**B**), αA (**C**) or εA (**D**).

ing an F-site, DHU, αA or εA reveals that all DNA substrates bound to the DNA-binding site in a similar manner with an extra-helical state of the F-site and damaged nucleotides (Supplementary Figure S6). A close-up view (Figure 7) indicates that the angle of nucleotide eversion is different for different lesions and seems to be associated with the correct location of the base in the pocket of the active site. The F-site and 2′-deoxyribose residues of DHU and εA nucleotides are close to each other, whereas in the pocket, the location of the adenine base in the α-anomer nucleotide requires an additional shift of the furanosyl residue into the depth of the enzyme by ∼1.6 Å. Moreover, in the active site, the plane of the adenine base is almost perpendicular to the plane of the εA base and the surface of the DHU base. Different modes of DNA damage location also lead to a shift of the scissile phosphodiester bond within 1.5 Å. These findings indicate that nucleotide binding site displays a high plasticity and is able to accommodate structurally different nucleotides.

Model structures of APE1–DNA complexes show that the pocket of the active site is formed by amino acid residues Asn-174, Asn-212, Asn-229, Ala-230, Phe-266 and Trp-280 (Figure 8 and Supplementary Figure S7). It should be noted that APE1 does not form any selective contacts with the damaged bases, which provide specificity of the enzyme to this particular DNA damage. These data explain the ability of APE1 to recognize chemically unrelated DNA lesions as an apparent plasticity of enzyme's active site. The comparison of distances between amino acid residues of the active site and various damaged nucleotides performed in the present study as well as with the data from the X-ray crystal structure of the APE1 complex with DNA containing an F-site (PDB ID: 5DFI, 30) support the conclusion that all damaged nucleotides are correctly oriented in the active site for the catalysed reaction (Supplementary Table S2 and Figure S8).

DISCUSSION

During the last three decades, many DNA repair enzymes have been investigated to understand how damaged DNA bases are sought and recognized among a large number of unmodified bases (50). Structural data have revealed that conformational changes in the enzyme and DNA play an important role in the recognition of specific substrates and may control the substrate specificity of enzymes. Nevertheless, to date, one of the urgent problems in the field of DNA repair has been the elucidation of the mechanisms ensuring high-accuracy recognition of damaged bases. Indeed, DNA repair enzymes such as DNA glycosylases and AP endonucleases, which are both able to recognize and remove damaged DNA bases, have completely different structures of the DNA-binding site and of the active site as well as amino acid residues involved in the specific recognition of the dam-

aged nucleotide and catalysis. On the other hand, practically all of them have common features when interacting with DNA substrates. For example, all DNA glycosylases (with the exception of some alkylpurine DNA glycosylases) and AP endonucleases with currently available structures bend DNA and flip out the damaged nucleotide from the double helix. Therefore, the DNA bending by enzymes seems to be an approach well suited to the initial recognition of a damaged DNA region. The increase in the flexibility of a DNA region owing to the lesion type could facilitate DNA bending in the course of enzyme binding (51). Moreover, numerous recent studies determined that DNA glycosylases 1D diffusively scan DNA using wedge amino acid residues to identify damaged nucleotides (52–62). In the catalytic complex, the damaged nucleotide is located in the pocket of the active site of the enzyme, where its final verification takes place. The void formed in the duplex after damage eversion is filled by some amino acid residues of the enzyme that stabilize the extra-helical nucleotide location and bent conformation of DNA.

Therefore, the common mechanism of damage recognition that provides high substrate specificity can be subdivided into a few steps: bending of damaged DNA by the enzyme, eversion of the damaged nucleotide from the double helix and verification of the damaged base in the active site of the enzyme by formation of specific contacts.

The ability of DNA to be bent by the enzyme is related to the flexibility of the double helix. A damaged nucleotide can increase flexibility of the double helix or even induce formation of stable curvature of DNA. Several studies have suggested that the abasic site increases flexibility of the DNA duplex (51,63,64). It has been reported that in some sequence contexts, increased flexibility in the region of the abasic site causes DNA bending at an angle of ∼20–30° (36,65). As determined by nuclear magnetic resonance (NMR) spectroscopy (our unpublished data) the non-planar DHU base destabilizes the double helix, thus resulting in a decrease of the melting temperature of the duplex in comparison with undamaged DNA. Such destabilization, also reported for several saturated pyrimidine bases (66), most likely leads to increased flexibility of the duplex. A solution structure of a DNA duplex containing a single αA also shows an 18° kink into the major groove at the lesion (67,68). On the other hand, the structures of duplexes containing a single εA show indicate that a damaged base induces only a local and relatively minor perturbation of the B-form conformation (69). Nevertheless, as revealed by NMR spectroscopy (70), εA destabilizes the double helix by significantly increasing the equilibrium constant of the base-opening process even in the complementary εA/T pair.

PELDOR and molecular dynamics data obtained for a set of DNA substrates here revealed that the F-site, αA and εA bases induced ∼20° DNA bending. Another modified base, DHU, induces two kinds of structural DNA changes. The first state with an increased end-to-end distance relative to an undamaged duplex indicates an increase of ∼2 Å in the internucleotide space because of intra-helical location of the non-planar DHU base. The second state with a significantly shortened end-to-end distance can be achieved via substantial DNA bending at an angle of ∼57°, probably with extra-helical location of the DHU nucleotide.

The detected DNA bending induced by the F-site, DHU, αA and εA nucleotides is suggestive of conformational flexibility of damaged DNA relative to the undamaged duplex. PELDOR analysis and molecular dynamics simulation revealed that APE1 induced significant additional DNA bending, decreasing in the order F-site ≈ DHU > αA > εA, which coincides with the efficiency of DNA substrate cleavage by APE1. Because the angle of DNA bending depends on duplex flexibility, which is related to the nature of the damage, it can be concluded that APE1 attempts to bend DNA until the damaged nucleotide flips out of the double helix into the active site of the enzyme. Model structures of the active site pocket revealed that the damage recognition by APE1 is not based on the formation of specific contacts with some structural elements of the damaged bases. Therefore, the substrate specificity should be controlled by the efficiency of damaged nucleotide eversion from the double helix during DNA bending induced by APE1.

Our stopped-flow FRET data suggest that the DNA bending stage proceeds after initial damage-dependent DNA distortion. The observed rate of this initial distortion process decreases in the same order as does the change in the bending angle: F-site ≈ DHU > αA > εA. It is reasonable to conclude that insertion of a nucleotide containing a damaged base into the active site of APE1 can be slower than the insertion of an abasic nucleotide because of possible steric inconvenience. The large εA base obviously has lower total efficiency of eversion from the double helix and of insertion into the active site. Indeed, our analysis of APE1 conformational changes by Trp fluorescence revealed that the observed rate constant of catalytic complex formation, which comprises both eversion from the duplex and insertion into the active site, decreases in the order corresponding to an increase in the size of the damaged base.

Therefore, our conclusion is that the ability of a damaged nucleotide to flip out from DNA and to penetrate the enzyme pocket—in the course of formation of contacts between DNA and the enzyme—may be the key contributing factor of substrate specificity of APE1. This conclusion is in good agreement with the ability of APE1 to act as an endoribonuclease due to the structural features of RNA that facilitate the eversion of intact nucleotides at the junction of the single-stranded parts, duplexes, hairpins, and loops. Moreover, it is reasonable to suggest that the formation of non-B-form DNA as well as sequence induced DNA flexibility are used by APE1 for undamaged nucleotide recognition and non-specific DNA cleavage.

SUPPLEMENTARY DATA

Supplementary Data are available at NAR Online.

FUNDING

Russian Government [VI.57.1.2, 0309-2016-0001, in part]; Russian Foundation of Basic Research Grant [16-04-00037]. The part of this work involving Trp and FRET detection combined with stopped-flow kinetics was

specifically funded by Russian Science Foundation grant [18-14-00135]. The part of this work involving PELDOR measurements was specifically funded by Russian Science Foundation grant [15-15-00021]. Funding for open access charge: Russian Science Foundation [18-14-00135].
Conflict of interest statement. None declared.

REFERENCES

1. Friedberg,E.C., Walker,G.C., Siede,W., Wood,R.D., Schultz,R.A. and Ellenberger,T. (2006) *DNA Repair and Mutagenesis*. ASM Press, WA, USA.
2. David,S.S. and Williams,S.D. (1998) Chemistry of glycosylases and endonucleases involved in base-excision repair. *Chem. Rev.*, **98**, 1221–1261.
3. Wilson,D.M. III and Barsky,D. (2001) The major human abasic endonuclease: formation, consequences and repair of abasic lesions in DNA. *Mutat. Res.*, **485**, 283–307.
4. Demple,B. and Sung,J.-S. (2005) Molecular and biological roles of Ape1 protein in mammalian base excision repair. *DNA Repair*, **4**, 1442–1449.
5. Barnes,D.E. and Lindahl,T. (2004) Repair and genetic consequences of endogenous DNA base damage in mammalian cells. *Annu. Rev. Genet.*, **38**, 445–476.
6. Gros,L., Saparbaev,M.K. and Laval,J. (2002) Enzymology of the repair of free radicals-induced DNA damage. *Oncogene*, **21**, 8905–8925.
7. Ischenko,A.A. and Saparbaev,M.K. (2002) Alternative nucleotide incision repair pathway for oxidative DNA damage. *Nature*, **415**, 183–187.
8. Prorok,P., Saint-Pierre,C., Gasparutto,D., Fedorova,O.S., Ishchenko,A.A., Leh,H., Buckle,M., Tudek,B. and Saparbaev,M. (2012) Highly mutagenic exocyclic DNA adducts are substrates for the human nucleotide incision repair pathway. *PLoS One*, **7**, e51776.
9. Christov,P.P., Banerjee,S., Stone,M.P. and Rizzo,C.J. (2010) Selective Incision of the alpha-N-Methyl-Formamidopyrimidine anomer by escherichia coli endonuclease IV. *J. Nucleic Acids*, **2010**, e850234.
10. Vrouwe,M.G., Pines,A., Overmeer,R.M., Hanada,K. and Mullenders,L.H. (2011) UV-induced photolesions elicit ATR-kinase-dependent signaling in non-cycling cells through nucleotide excision repair-dependent and -independent pathways. *J. Cell Sci.*, **124**, 435–446.
11. Guliaev,A.B., Hang,B. and Singer,B. (2004) Structural insights by molecular dynamics simulations into specificity of the major human AP endonuclease toward the benzene-derived DNA adduct, pBQ-C. *Nucleic Acids Res.*, **32**, 2844–2852.
12. Gros,L., Ishchenko,A.A., Ide,H., Elder,R.H. and Saparbaev,M.K. (2004) The major human AP endonuclease (Ape1) is involved in the nucleotide incision repair pathway. *Nucleic Acids Res.*, **32**, 73–81.
13. Daviet,S., Couve-Privat,S., Gros,L., Shinozuka,K., Ide,H., Saparbaev,M. and Ishchenko,A.A. (2007) Major oxidative products of cytosine are substrates for the nucleotide incision repair pathway. *DNA Repair*, **6**, 8–18.
14. Prorok,P., Alili,D., Saint-Pierre,C., Gasparutto,D., Zharkov,D.O., Ishchenko,A.A., Tudek,B. and Saparbaev,M.K. (2013) Uracil in duplex DNA is a substrate for the nucleotide incision repair pathway in human cells. *Proc. Natl. Acad. Sci. U.S.A.*, **110**, E3695–E3703.
15. Wilson,D.M. 3rd, Takeshita,M., Grollman,A.P. and Demple,B. (1995) Incision activity of human apurinic endonuclease (Ape) at abasic site analogs in DNA. *J. Biol. Chem.*, **270**, 16002–16007.
16. Strauss,P.R., Beard,W.A., Patterson,T.A. and Wilson,S.H. (1997) Substrate binding by human apurinic/apyrimidinic endonuclease indicates a Briggs-Haldane mechanism. *J. Biol. Chem.*, **272**, 1302–1307.
17. Gelin,A., Redrejo-Rodríguez,M., Laval,J., Fedorova,O.S., Saparbaev,M. and Ishchenko,A.A. (2010) Genetic and biochemical characterization of human AP endonuclease 1 mutants deficient in nucleotide incision repair activity. *PLoS One*, **5**, e12241.
18. Akishev,Z., Taipakova,S., Joldybayeva,B., Zutterling,C., Smekenov,I., Ishchenko,A.A., Zharkov,D.O., Bissenbaev,A.K. and Saparbaev,M. (2016) The major Arabidopsis thaliana apurinic/apyrimidinic endonuclease, ARP is involved in the plant nucleotide incision repair pathway. *DNA Repair (Amst).*, **48**, 30–42.
19. Timofeyeva,N.A., Koval,V.V, Knorre,D.G., Zharkov,D.O., Saparbaev,M.K., Ishchenko,A.A. and Fedorova,O.S. (2009) Conformational dynamics of human AP endonuclease in base excision and nucleotide incision repair pathways. *J. Biomol. Struct. Dyn.*, **26**, 637–652.
20. Timofeyeva,N.A., Koval,V.V, Ishchenko,A.A., Saparbaev,M.K. and Fedorova,O.S. (2011) Kinetic mechanism of human apurinic/apyrimidinic endonuclease action in nucleotide incision repair. *Biochemistry*, **76**, 273–281.
21. Timofeyeva,N.A. and Fedorova,O.S. (2016) A kinetic mechanism of repair of DNA containing alpha-anomeric deoxyadenosine by human apurinic/apyrimidinic endonuclease 1. *Mol. Biosyst.*, **12**, 3435–3446.
22. Miroshnikova,A.D., Kuznetsova,A.A., Vorobjev,Y.N., Kuznetsov,N.A. and Fedorova,O.S. (2016) Effects of mono- and divalent metal ions on DNA binding and catalysis of human apurinic/apyrimidinic endonuclease 1. *Mol. Biosyst.*, **12**, 1527–1539.
23. Masuda,Y., Bennett,R.A. and Demple,B. (1998) Rapid dissociation of human apurinic endonuclease (Ape1) from incised DNA induced by magnesium. *J. Biol. Chem.*, **273**, 30360–30365.
24. Gorman,M.A., Morera,S., Rothwell,D.G., de La Fortelle,E., Mol,C.D., Tainer,J.A., Hickson,I.D. and Freemont,P.S. (1997) The crystal structure of the human DNA repair endonuclease HAP1 suggests the recognition of extra-helical deoxyribose at DNA abasic sites. *EMBO J.*, **16**, 6548–6558.
25. Beernink,P.T., Segelke,B.W., Hadi,M.Z., Erzberger,J.P., Wilson,D.M. 3rd and Rupp,B. (2001) Two divalent metal ions in the active site of a new crystal form of human apurinic/apyrimidinic endonuclease, Ape1: implications for the catalytic mechanism. *J. Mol. Biol.*, **307**, 1023–1034.
26. Manvilla,B.A., Pozharski,E., Toth,E.A. and Drohat,A.C. (2013) Structure of human apurinic/apyrimidinic endonuclease 1 with the essential Mg2+ cofactor. *Acta Crystallogr. D Biol. Crystallogr.*, **69**, 2555–2562.
27. Mol,C.D., Izumi,T., Mitra,S. and Tainer,J.A. (2000) DNA-bound structures and mutants reveal abasic DNA binding by APE1 and DNA repair coordination. *Nature*, **403**, 451–456.
28. Mol,C.D., Hosfield,D.J. and Tainer,J.A. (2000) Abasic site recognition by two apurinic/apyrimidinic endonuclease families in DNA base excision repair: the 3′ ends justify the means. *Mutat. Res.*, **460**, 211–229.
29. Tsutakawa,S.E., Shin,D.S., Mol,C.D., Izumi,T., Arvai,A.S., Mantha,A.K., Szczesny,B., Ivanov,I.N., Hosfield,D.J., Maiti,B. *et al.* (2013) Conserved structural chemistry for incision activity in structurally non-homologous apurinic/apyrimidinic endonuclease APE1 and endonuclease IV DNA repair enzymes. *J. Biol. Chem.*, **288**, 8445–8455.
30. Freudenthal,B.D., Beard,W.A., Cuneo,M.J., Dyrkheeva,N.S. and Wilson,S.H. (2015) Capturing snapshots of APE1 processing DNA damage. *Nat. Struct. Mol. Biol.*, **22**, 924–931.
31. Kanazhevskaya,L.Y., Koval,V.V, Zharkov,D.O., Strauss,P.R. and Fedorova,O.S. (2010) Conformational transitions in human AP endonuclease 1 and its active site mutant during abasic site repair. *Biochemistry*, **49**, 6451–6461.
32. Kanazhevskaya,L.Y., Koval,V.V, Vorobjev,Y.N. and Fedorova,O.S. (2012) Conformational dynamics of abasic DNA upon interactions with AP endonuclease 1 revealed by stopped-flow fluorescence analysis. *Biochemistry*, **51**, 1306–1321.
33. Miroshnikova,A.D., Kuznetsova,A.A., Kuznetsov,N.A. and Fedorova,O.S. (2016) Thermodynamics of damaged DNA binding and catalysis by human AP endonuclease 1. *Acta Naturae*, **8**, 103–110.
34. Kuznetsova,A.A., Kuznetsov,N.A., Ishchenko,A.A., Saparbaev,M.K. and Fedorova,O.S. (2014) Pre-steady-state fluorescence analysis of damaged DNA transfer from human DNA glycosylases to AP endonuclease APE1. *Biochim. Biophys. Acta*, **1840**, 3042–3051.
35. Bradford,M.M. (1976) A rapid and sensitive method for the quantitation of microgram quantities of protein utilizing the principle of protein-dye binding. *Anal. Biochem.*, **72**, 248–254.
36. Kuznetsov,N.A., Milov,A.D., Koval,V.V., Samoilova,R.I., Grishin,Y.A., Knorre,D.G., Tsvetkov,Y.D., Fedorova,O.S. and Dzuba,S.A. (2009) PELDOR study of conformations of double-spin-labeled single- and double-stranded DNA with non-nucleotide inserts. *Phys. Chem. Chem. Phys.*, **11**, 6826–6832.

37. Milov,A.D., Grishin,Y.A., Dzuba,S.A. and Tsvetkov,Y.D. (2011) Effect of pumping pulse duration on echo signal amplitude in Four-Pulse PELDOR. *Appl. Magn. Reson.*, **41**, 59–67.
38. Jeschke,G., Chechik,V., Ionita,P., Godt,A., Zimmermann,H., Banham,J., Timmel,C.R., Hilger,D. and Jung,H. (2006) DeerAnalysis2006 - a comprehensive software package for analyzing pulsed ELDOR data. *Appl. Magn. Reson.*, **30**, 473–498.
39. Matveeva,A.G., Yushkova,Y.V., Morozov,S.V., Grygor'ev,I.A. and Dzuba,S.A. (2017) Multi-Gaussian Monte Carlo analysis of PELDOR data in the frequency domain. *Z. Phys. Chem.*, **231**, 671–688.
40. Matveeva,A.G., Nekrasov,V.M. and Maryasov,A.G. (2017) Analytical solution of the PELDOR inverse problem using the integral Mellin transform. *Phys. Chem. Chem. Phys.*, **19**, 32381–32388.
41. Kuznetsova,A.A., Kuznetsov,N.A., Ishchenko,A.A., Saparbaev,M.K. and Fedorova,O.S. (2014) Step-by-Step mechanism of DNA damage recognition by human 8-Oxoguanine DNA glycosylase. *Biochim. Biophys. Acta*, **1840**, 387–395.
42. Kuznetsova,A.A., Kuznetsov,N.A., Vorobjev,Y.N., Barthes,N.P.F., Michel,B.Y., Burger,A. and Fedorova,O.S. (2014) New environment-sensitive multichannel DNA fluorescent label for investigation of the protein-DNA interactions. *PLoS One*, **9**, e100007.
43. Vorobjev,Y.N. (2010) Blind docking method combining search of low-resolution binding sites with ligand pose refinement by molecular dynamics-based global optimization. *J. Comput. Chem.*, **31**, 1080–1092.
44. Popov,A.V., Vorobjev, and Y.N. (2010) GUI-BioPASED: a program for molecular dynamics simulations of biopolymers with a graphical user interface. *Mol. Biol.*, **44**, 735–742.
45. Cornell,W.D., Cieplak,P., Bayly,C.I., Gould,I.R., Merz,K.M., Ferguson,D.M., Spellmeyer,D.C., Fox,T., Caldwell,J.W. and Kollman,P.A. (1995) A second generation all atom force field for the simulation of proteins, nucleic acids and organic molecules. *J. Am. Chem. Soc.*, **117**, 5179–5197.
46. Wang,J.M., Cieplak,P. and Kollman,P.A. (2000) How well does a restrained electrostatic potential (RESP) model perform in calculating conformational energies of organic and biological molecules? *J. Comput. Chem.*, **21**, 1049–1074.
47. Wang,J.M., Wolf,R.M., Caldwell,J.W., Kollman,P.A. and Case,D.A. (2004) Development and testing of a general amber force field. *J. Comput. Chem.*, **25**, 1157–1174.
48. Lazaridis,T. and Karplus,M. (1999) Effective energy function for proteins in solution. *Proteins*, **35**, 133–152.
49. Kuznetsov,N.A., Milov,A.D., Isaev,N.P., Vorobjev,Y.N., Koval,V.V., Dzuba,S.A., Fedorova,O.S. and Tsvetkov,Y.D. (2011) PELDOR analysis of enzyme-induced structural changes in damaged DNA duplexes. *Mol. Biosyst.*, **7**, 2670–2680.
50. Brooks,S.C., Adhikary,S., Rubinson,E.H. and Eichman,B.F. (2013) Recent advances in the structural mechanisms of DNA glycosylases. *Biochim. Biophys. Acta*, **1834**, 247–271.
51. Marathias,V.M., Jerkovic,B. and Bolton,P.H. (1999) Damage increases the flexibility of duplex DNA. *Nucleic Acids Res.*, **27**, 1854–1858.
52. Dunn,A.R., Kad,N.M., Nelson,S.R., Warshaw,D.M. and Wallace,S.S. (2011) Single Qdot-labeled glycosylase molecules use a wedge amino acid to probe for lesions while scanning along DNA. *Nucleic Acids Res.*, **39**, 7487–7498.
53. Prakash,A., Doublie,S. and Wallace,S.S. (2012) The Fpg/Nei family of DNA glycosylases: substrates, structures, and search for damage. *Prog. Mol. Biol. Transl. Sci.*, **110**, 71–91.
54. Kuznetsova,A.A., Iakovlev,D.A., Misovets,I.V., Ishchenko,A.A., Saparbaev,M.K., Kuznetsov,N.A. and Fedorova,O.S. (2017) Pre-steady-state kinetic analysis of damage recognition by human single-strand selective monofunctional uracil-DNA glycosylase SMUG1. *Mol. Biosyst.*, **13**, 2638–2649.
55. Nelson,S.R., Dunn,A.R., Kathe,S.D., Warshaw,D.M. and Wallace,S.S. (2014) Two glycosylase families diffusively scan DNA using a wedge residue to probe for and identify oxidatively damaged bases. *Proc. Natl. Acad. Sci. U.S.A.*, **111**, E2091–E2099.
56. Kuznetsov,N.A., Kuznetsova,A.A., Vorobjev,Y.N., Krasnoperov,L.N. and Fedorova,O.S. (2014) Thermodynamics of the DNA damage repair steps of human 8-oxoguanine DNA glycosylase. *PLoS One*, **9**, e98495.
57. Chohan,M., Mackedenski,S., Li,W.M. and Lee,C.H. (2015) Human apurinic/apyrimidinic endonuclease 1 (APE1) has 3′ RNA phosphatase and 3′ exoribonuclease activities. *J. Mol. Biol.*, **427**, 298–311.
58. Kuznetsov,N.A., Kladova,O.A., Kuznetsova,A.A., Ishchenko,A.A., Saparbaev,M.K., Zharkov,D.O. and Fedorova,O.S. (2015) Conformational dynamics of DNA repair by escherichia coli endonuclease III. *J. Biol. Chem.*, **290**, 14338–14349.
59. Kuznetsov,N.A., Bergonzo,C., Campbell,A.J., Li,H., Mechetin,G.V., de los Santos,C., Grollman,A.P., Fedorova,O.S., Zharkov,D.O. and Simmerling,C. (2015) Active destabilization of base pairs by a DNA glycosylase wedge initiates damage recognition. *Nucleic Acids Res.*, **43**, 272–281.
60. Lee,A.J. and Wallace,S.S. (2016) Visualizing the search for Radiation-damaged DNA bases in real time. *Radiat. Phys. Chem. Oxf. Engl. 1993*, **128**, 126–133.
61. Lee,A.J. and Wallace,S.S. (2016) Hide and seek: How do DNA glycosylases locate oxidatively damaged DNA bases amidst a sea of undamaged bases? *Free Radic. Biol. Med.*, **107**, 170–178.
62. Kladova,O.A., Kuznetsova,A.A., Fedorova,O.S. and Kuznetsov,N.A. (2017) Mutational and Kinetic Analysis of Lesion Recognition by Escherichia coli Endonuclease VIII. *Genes (Basel)*, **8**, 1–13.
63. Chen,J., Dupradeau,F.Y., Case,D.A., Turner,C.J. and Stubbe,J. (2008) DNA oligonucleotides with A, T, G or C opposite an abasic site: structure and dynamics. *Nucleic Acids Res.*, **36**, 253–262.
64. Sicoli,G., Mathis,G., Aci-Seche,S., Saint-Pierre,C., Boulard,Y., Gasparutto,D. and Gambarelli,S. (2009) Lesion-induced DNA weak structural changes detected by pulsed EPR spectroscopy combined with site-directed spin labeling. *Nucleic Acids Res.*, **37**, 3165–3176.
65. Coppel,Y., Berthet,N., Coulombeau,C., Coulombeau,C., Garcia,J. and Lhomme,J. (1997) Solution conformation of an abasic DNA undecamer duplex d(CGCACXCACGC)-d(GCGTGTGTGCG): The unpaired thymine stacks inside the helix. *Biochemistry*, **36**, 4817–4830.
66. Lukin,M. and de Los Santos,C. (2006) NMR structures of damaged DNA. *Chem. Rev.*, **106**, 607–686.
67. Johnson,C.N., Spring,A.M., Desai,S., Cunningham,R.P. and Germann,M.W. (2012) DNA sequence context conceals alpha-Anomeric lesions. *J. Mol. Biol.*, **416**, 425–437.
68. Aramini,J.M., Cleaver,S.H., Pon,R.T., Cunningham,R.P. and Germann,M.W. (2004) Solution structure of a DNA duplex containing an alpha-anomeric adenosine: Insights into substrate recognition by endonuclease IV. *J. Mol. Biol.*, **338**, 77–91.
69. Kouchakdjian,M., Eisenberg,M., Yarema,K., Basu,A., Essigmann,J. and Patel,D.J. (1991) Nmr-Studies of the exocyclic 1, N(6)-Ethenodeoxyadenosine adduct (Epsilon-Da) opposite thymidine in a DNA Duplex - Nonplanar alignment of Epsilon-Da(Anti) and D\Anti) at the lesion site. *Biochemistry*, **30**, 1820–1828.
70. Kuznetsov,N.A., Kiryutin,A.S., Kuznetsova,A.A., Panov,M.S., Barsukova,M.O., Yurkovskaya,A.V. and Fedorova,O.S. (2017) The formation of catalytically competent enzyme-substrate complex is not a bottleneck in lesion excision by human alkyladenine DNA glycosylase. *J. Biomol. Struct. Dyn.*, **35**, 950–967.